ATLAS NOTE

ATLAS-CONF-2012-075

July 6, 2012

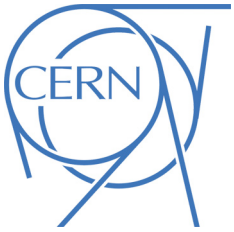

Searches for Heavy Long-Lived Sleptons and R-hadrons with the ATLAS Detector in pp Collisions at $\sqrt{s}$ = 7TeV

The ATLAS Collaboration

Abstract

A search for long-lived particles is performed using a data sample of 4.7 fb^{-1} from pp collisions at $\sqrt{s}$ = 7 TeV collected by the ATLAS detector at the LHC. No excess is observed above the estimated background and upper limits, at 95% CL, are set on the mass of the long-lived particles in different scenarios, based on their possible interactions in the inner detector, the calorimeters and the muon spectrometer. Long-lived staus in gauge-mediated SUSY breaking models are excluded up to a mass of 300 GeV for $\tan\beta = 5 - 20$. Directly produced long-lived sleptons are excluded up to a mass of 278 GeV. Gluino (stop, sbottom) *R*-hadrons in a generic interaction model are excluded up to a mass of 985 GeV (683 GeV, 612 GeV) respectively. Limits are also obtained for *R*-hadrons with a few ns lifetimes and on *R*-hadrons that do not reach the muon spectrometer or are neutral when they reach it.

ATLAS-CONF-2012-075
06 July 2012

1 Introduction

Heavy long-lived particles (LLPs) are predicted in a range of theories which extend the Standard Model (SM). Supersymmetry (SUSY) [1–9] models allow for long-lived charged sleptons ($\tilde{l}$), squarks ($\tilde{q}$) and gluinos ($\tilde{g}$). Heavy LLPs produced at the Large Hadron Collider (LHC) could travel with speed measurably lower than the speed of light. These particles can be identified and their mass, m, determined from their speed, β, and momentum, p, using the relation $m = p/\gamma\beta$. Four different searches are presented in this paper, using time of flight to measure β and specific ionisation energy loss, $\mathrm{d}E/\mathrm{d}x$, to measure $\beta\gamma$. The searches are optimised for the different experimental signatures of sleptons and composite colourless states of squarks or gluinos together with SM quarks and gluons, called *R*-hadrons.

Long-lived charged sleptons would interact like heavy muons, releasing energy by ionisation as they pass through the ATLAS detector. A search for long-lived sleptons identified in both the inner detector (ID) and in the muon spectrometer (MS) is therefore performed ("slepton search"). The results are interpreted in the framework of gauge-mediated SUSY breaking (GMSB) [10–16] with the light stau ($\tilde{\tau}$) as the LLP. In these models a substantial fraction of the events would contain two LLP candidates, and this feature is also utilised in discriminating signal from background.

Coloured LLPs ($\tilde{q}$ and $\tilde{g}$) would hadronise forming *R*-hadrons, bound states composed of the LLP and light SM quarks or gluons. They may emerge as charged or neutral states from the pp collision and be modified to a state with different charge by interactions with the detector material, arriving as neutral, charged or doubly charged particles in the muon spectrometer. Searches for *R*-hadrons are performed following three different approaches: using all available detector information ("full-detector *R*-hadron search"), ignoring the MS ("MS-agnostic *R*-hadron search") or using the inner detector alone ("ID-only *R*-hadron search"). The latter two cases aim to cover the lack of knowledge of *R*-hadron interactions with the detector and the possibility that their lifetimes do not allow them to reach the calorimeters.

Previous collider searches for LLPs have been performed at LEP [17–20], HERA [21], the Tevatron [22–28], and the LHC [29–35].

2 Data and simulated samples

The work presented in this paper is based on 4.7 fb^{-1} of pp collision data collected in 2011. The events are selected online by muon triggers for the slepton search and mainly by missing momentum triggers for the *R*-hadron searches. Data and Monte Carlo $Z \to \mu\mu$ samples are used for resolution studies. Monte Carlo signal samples, re-weighted for the distribution of pile-up events to match the running conditions of the 2011 data, are used to study the expected signal behaviour and to set limits.

The GMSB samples are generated with the following model parameters: number of super-multiplets in the messenger sector, $N_5 = 3$, messenger mass scale, $m_{\mathrm{messenger}} = 250$ TeV, sign of the Higgsino mass parameter, $\mathrm{sign}(\mu) = 1$, and C_{grav}, the scale factor for the gravitino mass which determines the NLSP life time was set to 5000 to ensure that the NLSP does not decay in the detector. The two Higgs doublets vacuum expectation values ratio, $\tan\beta$ varies between 5 and 40, and the SUSY particle mass scale values Λ varies from 50 to 150 TeV and the corresponding light $\tilde{\tau}$ masses from 122.2 to 465 GeV. The mass spectra of the GMSB models are obtained from the Spice program [36] and the events are generated using Herwig [37].

The *R*-hadron samples are generated with gluino (squark) masses from 300 to 1500 GeV (200 to 1000 GeV). The pair production of gluinos and squarks is simulated in Pythia [38], incorporating specialised hadronisation routines [39–41] to produce final states containing *R*-hadrons. A 10% gluino-ball fraction is assumed in the gluino sample production. The simulation of *R*-hadron interactions in matter is handled by dedicated Geant4 [42, 43] routines based on a generic model [44]. All Monte Carlo events pass the full ATLAS detector simulation [42, 45] and are reconstructed with the same programs as the

data. All signal Monte Carlo samples are normalised to the integrated luminosity of the data.

3 The ATLAS detector

The ATLAS detector [46] is a multipurpose particle physics detector with a forward-backward symmetric cylindrical geometry and near 4π coverage in solid angle[1]. The ID consists of a silicon pixel detector, a silicon micro-strip detector, and a transition radiation tracker. The ID is surrounded by a thin superconducting solenoid providing a 2 T magnetic field, and by high-granularity liquid-argon sampling electromagnetic calorimeters (LAr). An iron scintillator tile calorimeter provides hadronic coverage in the central rapidity range. The end-cap and forward regions are instrumented with liquid-argon calorimetry for both electromagnetic and hadronic measurements. The MS surrounds the calorimeters and consists of three large superconducting air-core toroids each with eight coils, a system of precision tracking chambers, and detectors for triggering.

ATLAS has a trigger system to reduce the data taking rate from up to 40 MHz to about 400 Hz, designed to keep the events that are potentially the most interesting. The first-level trigger (level-1) selection is carried out by custom hardware and identifies detector regions and a bunch crossing for which a trigger element is found. The high-level trigger is performed by dedicated software, seeded by data acquired from the bunch crossing and regions found at level-1. The components of particular importance to this analysis are described in more detail below.

3.1 The pixel detector

As the innermost detector system in ATLAS, the silicon pixel detector provides at least three precision measurements for each track in the region $|\eta| < 2.5$ at radial distances from the LHC beam line $r < 15$ cm. The sensors of the pixel barrel (covering the central $|\eta|$-region) are placed on three concentric cylinders around the beam-line, whereas sensors of the end-cap (covering the high $|\eta|$-region) are located on three disks perpendicular to the beam axis on each side of the barrel. In the barrel (end-cap) the intrinsic accuracy is 10 μm in the $r\phi$-plane and 115 μm in the $z(r)$-direction. When data are read out, the time for which the signal is above the threshold (ToT) is measured.

3.1.1 Pixel detector specific ionisation ($\mathrm{d}E/\mathrm{d}x$) measurement

The relation between ToT and the charge deposition in each pixel shows good linearity and stability as measured in dedicated calibration scans, enabling an energy loss measurement for charged particles with the pixel detector. The maximum ToT value corresponds to 8.5 times the average charge released by a minimum ionising particle (MIP) for a track perpendicular to the silicon detectors and leaving all its ionisation charge on a single pixel. If this value is exceeded, the ToT (and therefore the charge) is not correctly measured. Neighbouring pixels are joined together to form clusters and the charge of a cluster is calculated by summing up the charges of all pixels after calibration correction. The specific energy loss $\mathrm{d}E/\mathrm{d}x$ is defined as an average of the individual cluster charge measurements for the clusters associated with the track. To reduce the Landau tails, the average is evaluated after having removed the cluster with the highest charge (the two clusters with the highest charge are removed for tracks having five or more clusters).

[1] ATLAS uses a right-handed coordinate system with its origin at the nominal interaction point in the centre of the detector and the z-axis coinciding with the axis of the beam pipe. The x-axis points from the interaction point to the centre of the LHC ring, and the y-axis points upward. Cylindrical coordinates (r, ϕ) are used in the transverse plane, ϕ being the azimuthal angle around the beam pipe. The pseudo-rapidity is defined in terms of the polar angle θ as $\eta = -\ln\tan(\theta/2)$.

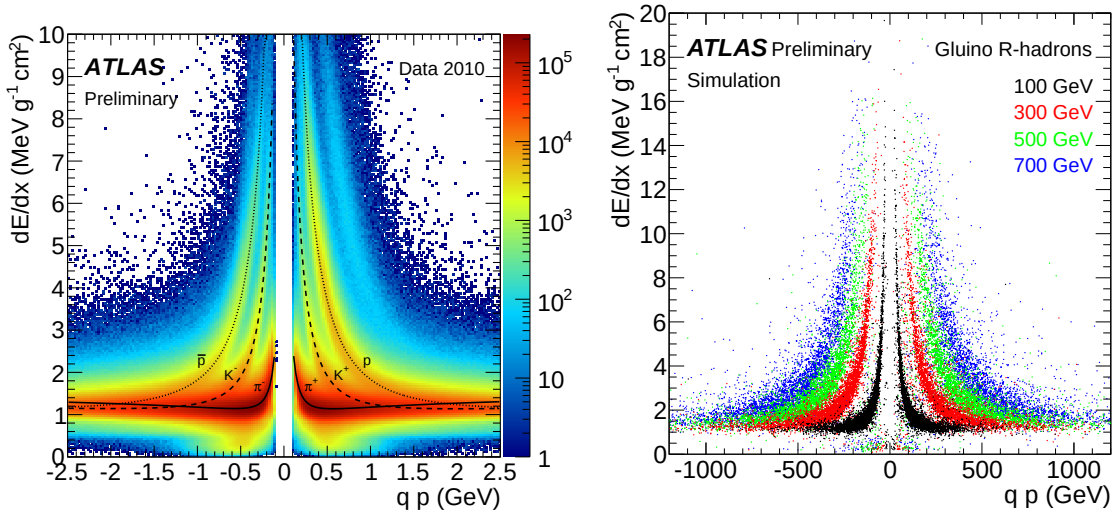

Figure 1: Left: Distribution of $\mathrm{d}E/\mathrm{d}x$ versus signed momentum for minimum bias collisions. In this data sample, from 2010 collisions, tracks are reconstructed down to 100 MeV p_{T} and therefore it is more suitable for Bethe-Bloch function calibration than 2011 data in which tracks had a cutoff of p_{T} =400 MeV. The distribution of the most probable value for the fitted probability density functions of pions (solid), kaons (dashed) and protons (dotted) are superimposed. Right: Simulated distribution of specific energy loss versus momentum for singly charged hypothetical R-hadrons of various masses.

3.1.2 Mass measurement with the pixel detector

The masses of slow charged particles can be measured using solely the ID information, i.e. by fitting each $\mathrm{d}E/\mathrm{d}x$ and momentum measurement to an empirical Bethe-Bloch function and deducing their $\beta\gamma$ value. The measurable $\beta\gamma$ range lies between 0.2 and 1.5; the lower bound being defined by the overflow in the ToT spectrum, and the upper bound by the overlapping distributions in the relativistic rise branch of the curve. This particle identification method, described in [47], uses a five-parameter function to describe how the most probable value of the specific energy loss ($\mathcal{M}_{\frac{\mathrm{d}E}{\mathrm{d}x}}$) depends on $\beta\gamma$:

$$\mathcal{M}_{\frac{\mathrm{d}E}{\mathrm{d}x}}(\beta\gamma) = \frac{p_1}{\beta^{p_3}} \ln(1 + (p_2\beta\gamma)^{p_5}) - p_4 \quad (1)$$

Figure 1 (left) shows how this function overlaps data for low momentum tracks. Figure 1 (right) shows the simulated pixel $\mathrm{d}E/\mathrm{d}x$ spectra for singly charged hypothetical R-hadrons of masses 100, 300, 500 and 700 GeV. As expected, these distributions extend into the high pixel $\mathrm{d}E/\mathrm{d}x$ region (pixel $\mathrm{d}E/\mathrm{d}x \gg 1$ MIP) even for high momentum tracks. The most probable value of $\mathrm{d}E/\mathrm{d}x$ for MIPs is about 1.2 MeVg^{-1}cm^2 with a spread of about 0.2 MeVg^{-1}cm^2 and a slight η dependence, increasing by about 10% from central to high η-regions.

For all tracks having a reconstructed momentum p and a measured specific energy loss $\mathrm{d}E/\mathrm{d}x$ above the value for MIPs, a mass estimate $m_{\beta\gamma} = p/\beta\gamma$ is obtained by inverting Equation 1.

The procedure is continuously monitored through precise ($< 1\%$) measurements of the mass of known particles (kaons and protons) and allows hypothetical heavy slow particles to be identified through their abnormal $\mathrm{d}E/\mathrm{d}x$ in a range of β of the order of $0.3 - 0.8$.

3.2 Calorimeters

Liquid argon is used as the active detector medium in the electromagnetic (EM) barrel and end-cap calorimeters, as well as in the hadronic end-cap (HEC) calorimeter. All are sampling calorimeters, using

lead plates for the EM calorimeters and copper plates for the HEC calorimeter. The EM calorimeters consist of accordion-shaped absorber. The barrel EM calorimeter covers the region $|\eta| < 1.475$ and consists of three layers and a pre-sampler. The EM end-cap calorimeter consists of three layers in the region $|\eta| < 2.5$ (two for $2.5 < |\eta| < 3.2$) and a pre-sampler for $|\eta| < 1.8$. The four layers of the HEC calorimeter cover the range $1.5 < |\eta| < 3.2$.

The ATLAS tile calorimeter is a cylindrical hadronic sampling calorimeter. It uses steel as the absorber material and plastic scintillators as the active layers. It covers radii from 2280 mm to 4230 mm while the η coverage extends to $|\eta| \lesssim 1.7$. The calorimeter is subdivided into a central barrel covering $|\eta| \lesssim 1.0$ and an extended barrel covering $0.8 \lesssim |\eta| \lesssim 1.7$. Both barrel parts are divided into 64 modules spaced evenly in azimuthal angle ϕ. The cells in each module are divided into three layers, which in the following analysis are all used both for the central and extended barrel.

3.2.1 Calorimeter β measurement

The ATLAS tile and LAr calorimeters have sufficiently good timing resolutions to distinguish highly relativistic SM particles from the slower moving LLPs. The time resolution depends on the energy deposited in the cell and also the layer type and thickness, but typical resolutions are 2 ns at 1 GeV, and generally better for the tile calorimeter.

To ensure the highest possible timing accuracy, it is necessary to calibrate the data using particles with known speed. It is then possible to correct the time-of-flight values such that they are in agreement with the known values. This calibration applies a common shift for each run, and is then performed as a function of calorimeter layer and cell energy. The reliability of such a calibration for this analysis depends on the assumption that the particles used for calibration have similar characteristics to the LLPs in question when depositing energy in the calorimeters. In the analysis muons are used for this purpose and it is cross checked that jets give a consistent result. The effect of small differences in time resolution as a function of arrival time, due to signal shaping, was tested by applying an arrival time dependent resolution function and found negligible. The β measurements from each cell on the extrapolated track are combined in a weighted average, typically using timing measurements from 3-4 calorimeter cells. The resolution of the resulting β measurement can be seen in Figure 2 (left).

3.3 The muon detectors

The MS forms the outer part of the ATLAS detector and detects charged particles exiting the calorimeters and measures their momenta in the pseudo-rapidity range $|\eta| < 2.7$. It is also designed to trigger on these particles in the region $|\eta| < 2.4$. The chambers in the barrel are arranged in three concentric cylindrical shells around the beam axis while in the two end-cap regions, muon chambers form three wheels, perpendicular to the z-axis.

The precision momentum measurement is performed by monitored drift-tube (MDT) chambers, using the η coordinate. These chambers consist of three to eight layers of drift tubes. In the forward region ($2 < |\eta| < 2.7$), Cathode-Strip Chambers are used in the innermost tracking layer. Resistive plate chambers (RPC) in the barrel region ($|\eta| < 1.05$), and thin gap chambers in the end-cap ($1.05 < |\eta| < 2.4$), deliver a fast level-1 trigger and measure both coordinates of the track, η and ϕ.

3.3.1 β measurement in the MS

The default reconstruction of particles in the MDT [48] relies on the assumption that they travel with the speed of light ($\beta = 1$). To improve the track quality for slow LLPs, the individual track segments can be reconstructed with different values for β. The actual β of the particle is estimated from the set of segments with the lowest χ^2. In a successive combined track re-fit, including ID and MS hits, the

particle trajectory is estimated more accurately. The time of flight to each tube is then obtained using the difference between the time of flight corresponding to the re-fitted track position in each tube and the time actually measured. By averaging the β's estimated from the time of flight in the different tubes an improved MDT β estimation can be achieved.

The RPC have an intrinsic time resolution of ~1 ns while the digitised signal is sampled with a 3.12 ns granularity, allowing a measurement of the time of flight. In the RPC, β is first calculated separately for each hit from the independent position and time measurements. A single β estimate is obtained by averaging the β's from all the hits.

The time of flight measurement quality is sensitive to the time resolution of the detector. By definition, in a perfectly calibrated detector, any energetic muon coming from a collision at the interaction point will pass the detector at $t_0 = 0$. The t_0 distributions in the different detector systems are measured and their means used to correct the calibration. The observed width of these distributions after correction is used as the error on the time measurement in the β fit and to smear times in the simulated samples. The time resolution in the MS does not depend on the arrival time.

3.4 Combining β measurements

There are three possible beta measurements per track, from the RPC, the MDT and the calorimeter. The β measurements from the different detectors are only used if $\beta > 0.2$ (the limit of the sensitivity) and if they are consistent internally, i.e. the χ^2 probability of the average between hits is reasonable (calorimeter) or the RMS of the measurement is consistent with the expected errors (MS). Measurements that are accepted are combined in a weighted average. The weights are obtained from the calculated error of each measurement, corrected for differences in the width of the pulls of the β distributions for muons from Z decay.

Since β is estimated from the measured time of flight, for a given resolution on the time measurement, a slower particle has a better β resolution. To simulate the time resolution correctly, the hit times in MC are smeared to reproduce the resolution measured in the data, prior to the β estimation. Figure 2 (right) shows the β distribution for selected $Z \to \mu\mu$ decays in data and MC with smeared hit times. The smearing mechanism reproduces the measured muon β distribution. The same time-smearing mechanism is applied to the signal Monte Carlo samples.

4 Event and candidate selection

4.1 Trigger selection

This analysis is based on events collected by two main trigger types: single muon and missing transverse momentum triggers.

4.1.1 Single muon trigger

The muon trigger and its performance in 2011 data are described in detail in [49]. This analysis uses un-prescaled muon triggers with a threshold of 18 GeV. Offline muons are selected with $p_{\mathrm{T}} > 50$ GeV, well above the trigger threshold.

Level-1 muon triggers are accepted and passed to the high-level trigger only if assigned to the collision bunch crossing. Late triggers due to late arrival of the particles are thus lost. The trigger efficiency for particles arriving late at the muon spectrometer is difficult to assess from data, where the majority of candidates are in-time muons. This efficiency is obtained from simulated R-hadron and GMSB events

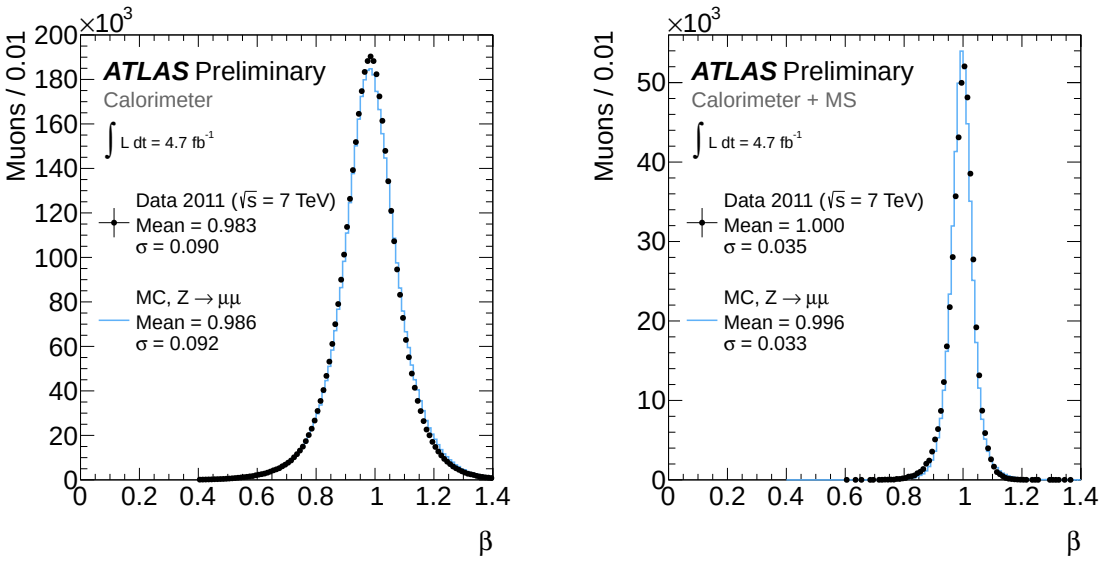

Figure 2: Distribution of β for the calorimeter (left) and combined measurements (right) obtained for selected $Z \to \mu\mu$ decays in data and MC simulation. The typical resolutions are quoted in the figures.

passing the Level-1 trigger simulation. The muon triggers are found to be efficient for GMSB signatures, which contain two typically high-β LLPs that reach the MS, and additional muons stemming from neutralino decays. The estimated trigger efficiency for GMSB slepton events is between 70% and 85%. Muon triggers are less efficient for R-hadron events, where neither or only one R-hadron may be charged as it enters the MS and β is typically low.

4.1.2 Missing transverse momentum trigger

Due to the strong nature of the gluino and squark production mechanism, R-hadron events often contain high p_{T} jets from QCD radiation. The modest energy depositions of the R-hadrons themselves combined with these jets naturally give rise to missing transverse momentum ($E_{\mathrm{T}}^{\mathrm{miss}}$).

The R-hadron analyses use un-prescaled missing transverse momentum triggers with thresholds between 60 GeV and 70 GeV evaluated at the electromagnetic energy scale (for the full-detector search the single muon trigger is used as well). Unlike the muon trigger, there is no loss of efficiency for the $E_{\mathrm{T}}^{\mathrm{miss}}$ triggers when R-hadrons arrive late. Their efficiency decreases with increasing mass as the gg-fusion production fraction decreases, though it remains between 15% and 20% for heavy R-hadrons.

4.2 Offline selection

Two different signal types are studied: sleptons and R-hadrons. Given the different expected signal interactions with the ATLAS detector, two dedicated candidate and event selections are used as described in the following. A candidate is a track considered as an LLP candidate.

4.2.1 Common event selection

Collision events are selected by requiring a good primary vertex with at least three ID tracks, and with requirements on the position of the reconstructed primary vertex. Events flagged as having flaws in detector operation are rejected. Cosmic ray background is rejected by removing tracks that do not pass close to the primary vertex in z. Candidates with an ID track with $|z_0^{\mathrm{trk}} - z_0^{\mathrm{vtx}}| > 10$ mm are removed,

where z_0^{trk} is the z coordinate at the distance of closest approach of the track to the primary vertex. For the analyses involving the muon spectrometer, events with cosmic rays are also rejected by a topological cut on any two candidates with opposite η and ϕ ($|\eta_1 + \eta_2| < 0.005$ and $||\phi_1 - \phi_2| - \pi| < 0.005$).

4.2.2 Slepton candidate selection

The analysis searching for sleptons requires two muon candidates in each event, because two sleptons are produced, and both have a high probability of being observed in the MS. Two sets of selection criteria are applied. A loose selection with high efficiency is used to select candidates in events where there are two LLP candidates. Very rarely would a non-GMSB event have two high p_{T} muons with poorly measured β and a large reconstructed mass. In events where only one candidate passes the loose selection, that candidate is required to pass a tight selection.

Candidates in the loose slepton selection are required to have $p_{\text{T}} > 50$ GeV. The p_{T} measurements in the ID and MS are required to be consistent, and the difference between them should not exceed a half of their average. Each candidate is required to have $|\eta| < 2.5$. Any two candidates that combine together to give an invariant mass close to the Z mass (± 10 GeV) are both rejected. Candidates are also required to have associated hits in at least two of the three main muon layers.

The estimated β is required to be consistent for measurements in the same detector system, based on the hit time resolutions. The number of calorimeter cells and MS hits contributing to the β measurement must exceed the number of detector systems used by three. For signal, low β values should be consistent between measurements whereas for muons they are the result of poor estimation and should be inconsistent between measurements. Therefore the β measurements from the different detector systems are required to be consistent with each other. The different detector system measurements of β are required to be pair-wise consistent at the 3σ level, and the combined β to be consistent with the $\beta\gamma$ estimated in the pixel within 3σ. Finally, in order to reduce the muon background, the combined β measurement is required to be less than 0.95.

To pass the tight selection, a candidate is required in addition to have $p_{\text{T}} > 70$ GeV, at least two separate detector systems measuring β, the number of hits minus the number of detector systems participating in the measurement at least twelve, and the consistency between β estimates in different detector systems has to be within 2σ. These cuts are optimised to give better background rejection.

Finally, a mass cut is applied on the candidate mass, $m_\beta = p/\gamma\beta$, calculated from the candidate's momentum and its measured β. This cut depends on the hypothetical $\tilde{\tau}$ mass and is different for different GMSB models, determined by the expected significance of the signal. For the two candidate sample, both masses are required to be above the cut. The number of background and expected signal events above the mass cut in the two-candidate and one-candidate signal regions is used to obtain the exclusion limit.

Typical efficiencies for signal events to pass all cuts including the mass cut are 20% for each of the one and two candidate event categories, giving 40% efficiency in total.

4.2.3 *R*-hadron candidate selection

Since the *R*-hadron contains light quarks in addition to the squark or gluino, the charge of the *R*-hadron can change following nuclear interactions with the detector material. This possibility makes it difficult to rely on a single detection mechanism without some loss of detection efficiency, as a neutral state would go undetected until the next nuclear interaction occurs. Some of the main hadron states considered in the models considered are neutral, and it is thus natural to take an inside-out approach, starting from the ID track and adding discriminators from outer detector systems, if a signal is seen along the extrapolated track. This is reflected in the three different *R*-hadron searches; "full-detector", "MS-agnostic" (not considering the MS) and "ID-only" (relying solely on the ID); making successively fewer assumptions

about the R-hadron scattering model and lifetime. While the first two differ only by their estimate of β (the "MS-agnostic" uses only the calorimeters) and the utilised triggers, the latter selection is generally more restrictive, to reject the larger backgrounds.

In the full-detector and MS-agnostic analysis, R-hadron candidates are required to have a good quality ID track with $p > 140$ GeV and $|\eta| < 2.5$. The track should not be within an $\eta - \phi$ distance $\Delta R < 0.3$ of any jet with $p_{\mathrm{T}} > 40$ GeV, reconstructed using the anti-k_t jet algorithm [50] and radius set to 0.4. Furthermore, track should not have any nearby ($\Delta R < 0.25$) tracks with $p_T > 10$ GeV nor pixel hits shared with another track. Tracks with momenta greater than 3.5 TeV are rejected as unphysical. The candidate should have a good $\mathrm{d}E/\mathrm{d}x$ measurement and a good estimate of β. The uncertainty on β is required to be less than 10% when measured with the calorimeter only, and less than 4% when the result of a combination.

In the ID-only analysis, selection requirements are further tightened. Vertices must have more than four tracks associated and the $E_{\mathrm{T}}^{\mathrm{miss}}$ trigger must be confirmed off-line ($E_{\mathrm{T}}^{\mathrm{miss}} > 85$ GeV) to ensure better background rejection. Candidate R-hadron tracks should have more than two (six) pixel (SCT) hits, impact parameters compatible with the primary vertex, $p_{\mathrm{T}} > 50$ GeV and $p > 100$ GeV. The isolation cut is also more severe rejecting events with tracks of p_T above 1 GeV within $\Delta R < 0.25$. Additionally, tracks are disregarded if their momentum resolution exceeds 50%, or if they can be identified as an electron.

About 8% of the data events have more than one candidate passing this selection (20% for signal MC). In the ID-only analysis there are no double candidate events in data (10% in MC). In the double-candidate events, only one candidate is used, chosen at random.

The final signal selection in the full-detector and MS-agnostic analysis is based on requirements on $\beta\gamma$ and β, optimised for each mass hypothesis, but generally ranges from $\beta\gamma < 1.5 - 2.0$ and $\beta < 0.8 - 0.9$ with lower values for higher masses. The signal region is defined in the $m_{\beta\gamma}$-m_{β} plane as 2σ below the mass peak and up to 2.5 TeV in each of the two mass estimates. For the ID-only analysis the final selection is based solely on exceeding a $\mathrm{d}E/\mathrm{d}x$ threshold which is set such as to reject MIPs uniformly in the η range. The selection efficiency for gluino R-hadrons of 900 GeV mass is about 11% and 7% in the full-detector and MS-agnostic analyses, respectively. It is about 6% in the ID-only analysis.

An alternative R-hadron model, which is an extension of the triple-Regge model used to describe squark R-hadrons [44] has also been considered. In this model, the signal efficiency is 40% lower at 300 GeV and increasing to the same level at 900 GeV above which it is higher, compared to the model used throughout this analysis.

5 Background estimation

The background for both the slepton and the R-hadron searches is mostly composed of high-p_{T} muons with mis-measured β, or in the case of the ID-only analysis, high p_{T} tracks with mismeasured $\mathrm{d}E/\mathrm{d}x$. The background estimation is derived from data in all cases.

The estimation of the background mass distributions relies on two assumptions: that the signal to background ratio before applying cuts on β is small, and that the β distribution for background candidates is due to measurement resolution and is therefore independent of the source of the candidate and its momentum. Checks of the validity of these assumptions are discussed in section 6.3.

The detector is divided into η regions so that the β resolution within each region is similar. The muon-β probability density function (PDF) in each η region is the distribution of the measured β of all muons in the region normalized to one. The sample used in producing the β PDF is enlarged with respect to the main selection of the analysis by lowering the p_{T} cut to 30 GeV and removing the Z veto, in order to increase the statistics and reduce possible signal contamination. Similarly, a $\beta\gamma$ PDF is constructed from tracks in a background dominated region.

The reconstructed mass distribution of muons in different regions of the detector depends on both β and momentum distributions through $m = p/\gamma\beta$. The regions also differ in the muon momentum distribution, therefore the combination of momentum with random β (see below) is done separately in each region and the resulting mass distributions are added together.

5.1 Slepton search

For each candidate passing the candidate selection described above, but without the cuts on the value of β or the mass, a random β is drawn from the muon-β PDF. If this β passed the selection, a mass is calculated using the reconstructed momentum of the candidate and this β value. The statistical error of the background estimate is reduced by repeating the procedure many times for each candidate and dividing the resulting distribution by the number of repetitions. The distribution of mass obtained this way gives the background estimate. The estimated background combined across all regions is shown for events containing two loose candidates in Figure 3 (top-left). The minimum mass of the two candidates is shown.

5.2 *R*-hadron searches

For the *R*-hadron full-detector and MS-agnostic analysis, all three of momentum, $\beta\gamma$ and β are obtained by randomly sampling distributions derived from data and combined to form mass estimates. The mass distributions are then normalised to data by scaling to a sideband outside the signal region.

For the ID-only analysis the choice of the control sample takes into account the non-negligible correlations between p, $\mathrm{d}E/\mathrm{d}x$ and η. The ionisation dependence on the path length in the sensor is not linear [51], so the pixel $\mathrm{d}E/\mathrm{d}x$ depends on η; the ionisation also depends on the particle $\beta\gamma$ via the Bethe-Bloch formula and therefore on its momentum, until the Fermi plateau is reached; finally p and η are kinematically dependent. Two background samples are used to derive the distributions which are used for the random-sampling. These two samples are derived by going back to a more inclusive sample. Both selections use the full data sample, but ensure that signal contamination is minimised.

- A first sample ("low-ionisation") is used to generate the η and p distributions. This is selected in the same way as the event candidates, but without the requirement on high ionisation. Instead, an upper threshold cut is placed on the $\mathrm{d}E/\mathrm{d}x$ (at (1.8 $\mathrm{MeVg^{-1}cm^2}$)), ensuring orthogonality with the signal selection.

- A second background sample ("low-momentum") is used to generate the $\mathrm{d}E/\mathrm{d}x$ templates. A background sample free of signal but with no upper limit on the $\mathrm{d}E/\mathrm{d}x$ is obtained by considering tracks that have a maximum momentum of 100 GeV. Specifically tracks in the "low-momentum" background sample satisfy all the event candidate requirements except that the transverse momentum cut is looser, $p_{\mathrm{T}} > 10$ GeV, and the momentum p is required to be between 40 and 100 GeV (where the Fermi plateau has already been reached).

A high-statistics background sample consisting of two million p, η, $\mathrm{d}E/\mathrm{d}x$ triplets is randomly generated. The momentum is first generated according to a binned function based on "low-ionisation" events. Then the pseudo-rapidity is generated according to the $\eta(p)$ binned functions based on "low-ionisation" events. Finally the ionisation is generated according to $\mathrm{d}E/\mathrm{d}x(\eta)$ binned functions based on "low-momentum" events. The normalisation of the generated background to the selected data is obtained by scaling the background to the data before the high $\mathrm{d}E/\mathrm{d}x$ cut and in the region of the mass distribution where no signal is expected (mass below 140 GeV).

6 Systematic uncertainties

Several possible sources of systematic effects are studied. The resulting systematic uncertainties are summarised in Table 1. The errors given are those on the expected yields in the signal region.

6.1 Theoretical cross-sections

Signal cross sections are calculated to next-to-leading order in the strong coupling constant, including the resummation of soft gluon emission at next-to-leading-logarithmic accuracy (NLO+NLL) [52–54][2]. The nominal cross section and its uncertainty are taken from an envelope of cross section predictions using different parton distribution function sets and factorisation and renormalisation scales, as described in [56]. This prescription leads to a 5% relative uncertainty on the expected signal normalisation in the slepton search, and a 15% to 30% uncertainty for the *R*-hadron search, increasing with *R*-hadron mass.

6.2 Expected signal

The muon trigger efficiency is calculated using the tag-and-probe technique on Z events as described in [49]. The uncertainty on the single muon trigger efficiency is estimated to be 1%. The reduction in the muon trigger efficiency due to late arrival of particles is estimated from simulation. The effect of the difference between data and MC in time alignment of hits in the muon trigger system relative to the LHC clock is estimated by shifting the hit time of the highest β candidate in each simulated event by 4 ns. The difference in trigger efficiency when this change is applied is between 0.5% and 1.5% for the different GMSB samples, and a systematic uncertainty of 1.5% is assigned. For *R*-hadrons the systematic uncertainty is estimated in the same way and found to be 2%.

The $E_{\mathrm{T}}^{\mathrm{miss}}$ trigger used for the *R*-hadrons relies on the emission of jets. Therefore, the trigger efficiency depends on the amount of initial and final state radiation (ISR and FSR) and the uncertainties on them. To evaluate the uncertainty, 1 TeV gluino pair production samples are simulated in Pythia 6.4.26 using the Perugia 2011 tune [57] setting the radiation level low and high. A simple threshold curve modelling of the trigger is applied to all three samples. The largest variation from the central sample is found to be 8.5%.

The $E_{\mathrm{T}}^{\mathrm{miss}}$ triggers use calorimeter energy deposits to calculate the transverse energy, and are thus blind to muons, which therefore can be used for calibration and to study systematic errors. To evaluate the trigger efficiency, the trigger turn-on curve is obtained by fitting the measured efficiency vs. $E_{\mathrm{T}}^{\mathrm{miss}}$ in $Z \to \mu\mu$ events where the Z has a high p_{T}, both in data and simulation. These efficiency turn-on curves are then applied to the expected $E_{\mathrm{T}}^{\mathrm{miss}}$ spectrum from simulated *R*-hadron events. The total uncertainty is estimated from three contributions: the relative difference between the efficiencies obtained using the fitted threshold curve from $Z \to \mu\mu$ data and simulation and the difference in efficiencies obtained from independent $\pm 1\sigma$ variations in fit parameters relative to the unchanged onset fit for both $Z \to \mu\mu$ data and MC. The total estimated $E_{\mathrm{T}}^{\mathrm{miss}}$ trigger uncertainty, including effects of a 10% variation of the $E_{\mathrm{T}}^{\mathrm{miss}}$ scale, is a 4.5% relative error on the efficiency for the signal.

The effect in the ID-only analysis on the total efficiency of the uncertainty on the $E_{\mathrm{T}}^{\mathrm{miss}}$ measurement has been evaluated by applying a scale factor of ± 10% and a smearing up to 20% to the missing energy [58]. The resulting uncertainty depends on the *R*-hadron mass and is within 7.3% (200 GeV) and 4.5% (1500 GeV) of the central value.

[2]The NLL correction is used for squark and gluino production when the squark and gluino masses lie between 200 GeV and 2 TeV. Following the convention used in the NLO calculators the squark mass is defined as the average of the squark masses in the first two generations. In the case of gluino-pair (associated squark-gluino) production processes, the NLL calculations are extended up to squark masses of 4.5 TeV (3.5 TeV). For masses outside this range and for other types of production processes (i.e. electroweak and associated strong and electroweak) cross-sections at NLO accuracy obtained with Prospino [55] are used.

Differences in the selection efficiency between data and MC for the R-hadron full-detector and MS-agnostic searches (excluding the final selection on $\beta\gamma$, β, momentum and mass selection) are evaluated using $Z \rightarrow \mu\mu$ events. The overall relative uncertainty is found to be below 1.5%. The systematic uncertainty of the jet energy scale (JES) on the requirement for signal candidates in the R-hadron full-detector and MS-agnostic searches to be away from jets with $p_{\mathrm{T}} > 40$ GeV is found to be negligible.

To verify that the signal efficiency is insensitive to the pile-up re-weighting, a 900 GeV gluino sample is divided into samples of high ($N_{\mathrm{vtx}} \geq 8$) and low ($N_{\mathrm{vtx}} < 8$) number of reconstructed primary vertices. The relative difference in reconstruction efficiency is found to be negligible.

The systematic uncertainty due to the track reconstruction efficiency and momentum resolution differences between data and simulation is estimated [59] to be 0.5% for GMSB events. For analyses relying solely on the ID for tracking, the resulting relative uncertainty on the signal efficiency is 1.3%.

Differences in the pixel $\mathrm{d}E/\mathrm{d}x$ and the subsequent measurement of $\beta\gamma$ between data and simulation are considered by comparing the pixel $\mathrm{d}E/\mathrm{d}x$ distribution for high-p_{T} muons from $Z \rightarrow \mu\mu$ events in data and MC. This uncertainty is estimated to be 5%.

The signal β resolution is estimated by smearing the measured time of hits in the MS and calorimeter according to the spread observed in the time calibration. The systematic uncertainty due to the smearing process is estimated by scaling the smearing factor up and down, so as to bracket the distribution obtained in data. A 4% (6%) systematic uncertainty is found in the one-candidate (two-candidate) GMSB signal region. The corresponding uncertainty for R-hadrons is 3.6%. The uncertainty due to the timing calibration of the calorimeter hits is further tested by comparing a calibration obtained from jet events to that obtained from muons. This results in a 1% relative systematic uncertainty on the signal yield.

An uncertainty of 3.9% [60, 61] is assigned to the integrated luminosity represented by the dataset.

6.3 Background estimation

The total uncertainty on the background estimate for the slepton search is 13% for two-candidate events and 11% for one-candidate events. To test the momentum dependence of the muon β PDF, the candidates in each η region are divided by their momentum into two bins with similar counts, and the background estimated with the resulting β PDFs. The resulting uncertainty on the slepton search is 10%. To quantify the variability of the β and momentum distributions within a region and its effect on the background estimation for sleptons, the detector is sub-divided into 25 η regions instead of the eight used in the analysis and the background estimated with this division. The resulting systematic uncertainty is 6.5% for the two-candidate events and 3.1% for one-candidate events. The uncertainty on the background distribution coming from the limited statistics of the data samples used to estimate the momentum distribution was calculated by dividing the candidate sample randomly into two samples and estimating the background from each sub-sample separately. The resulting error in the slepton search is negligible. A comparison of the β distribution of inclusive muon events to that from Z decays also exhibited negligible differences.

The total uncertainty in the background estimation for the full-detector R-hadron analysis is estimated as follows. The $\beta\gamma$ and β PDFs are obtained by considering sidebands (lower momenta, for R-hadrons typically 40-100 GeV). Similarly, the momentum PDF is obtained from sidebands in either/or $\beta\gamma$ and β. The size of the sidebands is varied in several ways (also to include the signal region), which resulted in $8 - 10\%$ uncertainties for each of the two variables. To test the momentum dependence of the β PDF, the number of η bins is varied. The resulting systematic uncertainty is 2%. To estimate the uncertainty on the background distribution coming from the limited statistics of the data samples used to estimate the momentum distribution, the candidate sample is divided randomly into two samples and the background estimate derived from each sub-sample separately. The resulting uncertainty on the full detector R-hadron search is 2% for low mass and 5% for high mass.The total uncertainty on the background estimate from the above tests is 15%.

Source	GMSB sleptons		R-hadrons	
	one-cand.	two-cand.	ID-only	other
Theoretical systematic uncertainty on signal size	5	5	15–30	
Uncertainty on signal efficiency				
Signal trigger efficiency	1.8	1.8	4.5	4.5
QCD uncertainties (ISR, FSR)			8.5	8.5
Signal pre-selection efficiency				1.5
Momentum resolution	0.5	0.5	1.3	1.3
Pixel $\mathrm{d}E/\mathrm{d}x$ calibration			5.8–0.2	5
Combined β timing calibration	4	6		
Calo β timing calibration				1.0
MS β timing calibration				3.6
Offline $E_{\mathrm{T}}^{\mathrm{miss}}$ scale			7.3–4.5	
Total uncertainty on signal efficiency	4.4	6.3	13.4–10.6	11.6
Luminosity	3.9	3.9	3.9	3.9
Experimental uncertainty on background estimate	11	13	3–20	15

Table 1: Summary of systematic uncertainties (given in percent). Ranges indicate a mass dependence for the given uncertainty.

For the ID-only analysis, the statistical uncertainty in the background estimate dominates for most of the mass range, and is up to 20%. Other effects contribute at most a few percent. These include variations from different binning choices for p, eta and dE/dx in the two background samples, and a contribution of 2.5% from pile-up effects.

7 Results

The mass distributions observed in data together with the background estimate, its systematic error and examples of signal are shown in Figure 3, for the two-candidate signal region in the slepton search (top-left), the full-detector R-hadron search (top-right), the MS-agnostic R-hadron search (bottom-left) and the ID-only R-hadron search (bottom-right).

No indication of signal above the expected background is observed, and limits on new physics scenarios are set by counting the number of events passing a set of model-dependent mass cuts. Cross-section limits are obtained using the CL_s prescription [62]. Mass limits are derived by comparing the obtained cross-section limits to the lower edge of the 1σ band around the theoretically predicted cross-section for each process. A Poisson likelihood function is used for the R-hadron limit setting while a likelihood combining two Poisson functions is used for the slepton search to benefit from the separation into one-candidate and two-candidate signal regions.

The resulting production cross-section limits in the GMSB scenario as a function of the stau mass are presented in Figure 4 and compared to theoretical predictions. Long-lived staus in GMSB models with $N_5 = 3$, $M_{\mathrm{messenger}} = 250$ TeV and $\mathrm{sign}(\mu) = 1$ are excluded at 95% CL up to a stau mass of 300 GeV for $\tan\beta = 5 - 20$, and up to stau masses of 285 GeV and 268 GeV for $\tan\beta = 30$ and $\tan\beta = 40$. The lower limit on Λ is $99 - 110$ TeV for values of $\tan\beta$ from 5 to 40. For Λ values around this limit, strong production of squarks and gluinos is suppressed due to their large masses. Directly produced sleptons comprise $38\% - 64\%$ of the GMSB cross-section, and depend only on the slepton mass. Using the same analysis as for GMSB, directly produced long-lived sleptons are excluded at 95% CL up to slepton

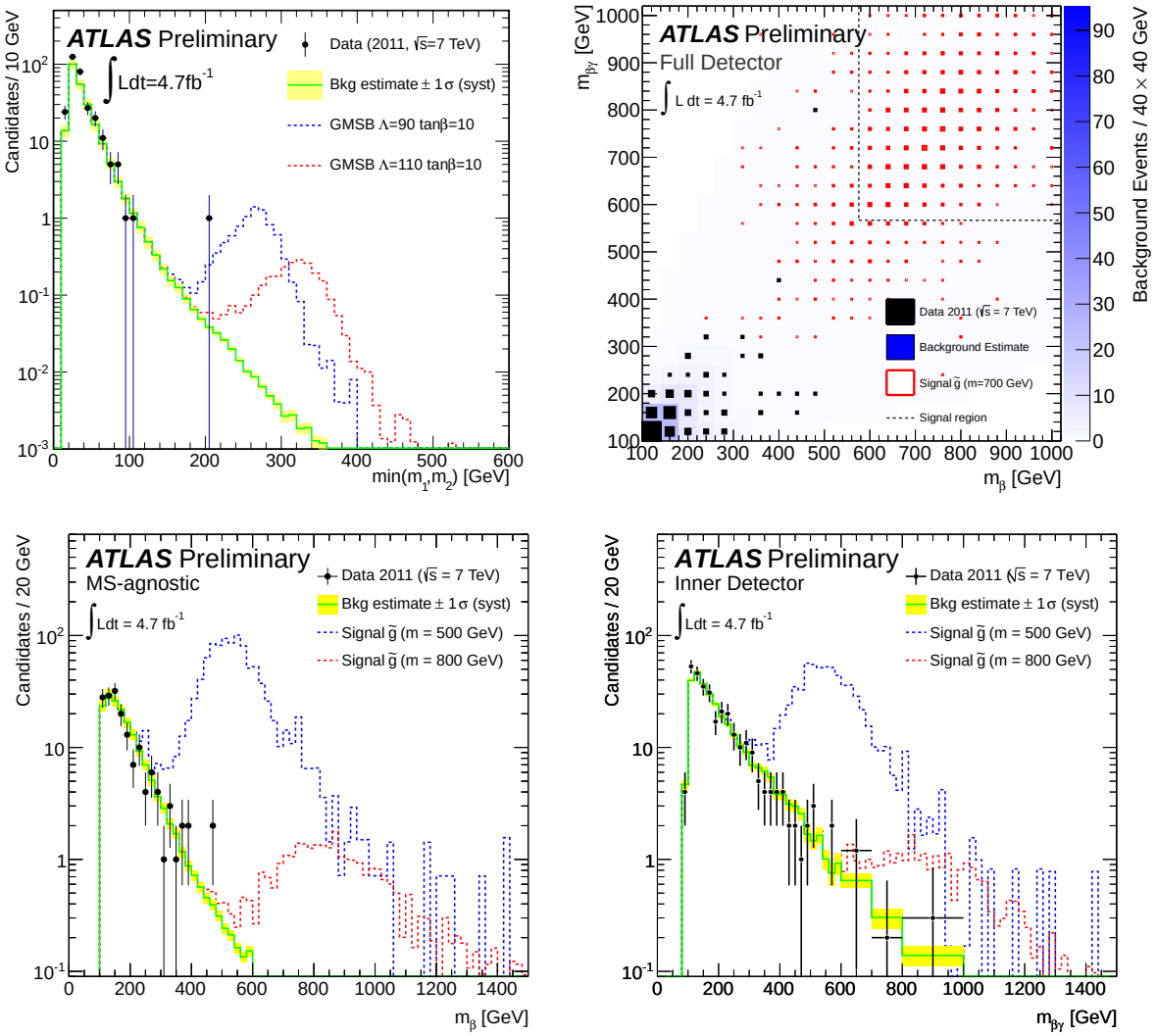

Figure 3: Observed data, background estimate and expected signal in the two-candidate signal region in the slepton search (top-left), full detector *R*-hadron search (top-right), MS-agnostic *R*-hadron search (bottom-left) and in the ID-only *R*-hadron search (bottom-right). The m_β-distribution for the MS-agnostic *R*-hadron search (bottom-left) is shown, for illustration purposes, after all but the mass selection requirement applied.

masses of 278 GeV.

The resulting limits on R-hadrons are shown in Figures 5 and 6 compared to the theoretical cross-sections. Gluino R-hadrons in a generic interaction model are excluded up to a mass of 985 GeV. Stop R-hadrons are excluded up to a mass of 683 GeV, and sbottom R-hadrons are excluded up to a mass of 612 GeV. For R-hadrons hadronising into neutral bound states before reaching the muon spectrometer, the MS-agnostic search yields a lower mass limit of 989 GeV for gluinos, 657 GeV for stops and 618 GeV for sbottoms. The limits from the ID-only search are shown in Figure 7 compared to the theoretical cross-sections. Gluino R-hadrons with $m < 940$ GeV, stop R-hadrons with $m < 604$ GeV and sbottom R-hadrons with $m < 576$ GeV are excluded at 95% CL. As the ID-only search is sensitive also to R-hadrons with a few ns lifetime with similar selection efficiency, those are also excluded in the same mass range.

8 Conclusion

Searches for long-lived massive particles were performed using data from pp-collisions at $\sqrt{s} = 7$ TeV collected by the ATLAS detector in 2011, corresponding to a luminosity of 4.7 fb^{-1}. Several different signatures are considered. The data are found to match the Standard Model background expectation in all signal regions. The exclusion limits placed for various models impose new constraints on non-SM cross-sections. Long-lived staus in the GMSB model considered, for $\tan\beta = 5 - 20$, are excluded at 95% confidence level (CL) for masses up to 300 GeV, while directly produced long-lived sleptons are excluded up to 278 GeV.

Long-lived R-hadrons containing a gluino (stop, sbottom) are excluded for masses up to 985 GeV (683 GeV, 612 GeV) at 95% CL, for a generic interaction model. Furthermore, using only the inner detector, R-hadrons are excluded up to 940 GeV (604 GeV, 576 GeV). R-hadrons which may be neutral by the time they reach the muon spectrometer are excluded up to masses of 989 GeV (657 GeV, 618 GeV).

These results substantially extend previous ATLAS limits [32, 33], and are largely complementary to the searches for SUSY particles which decay promptly.

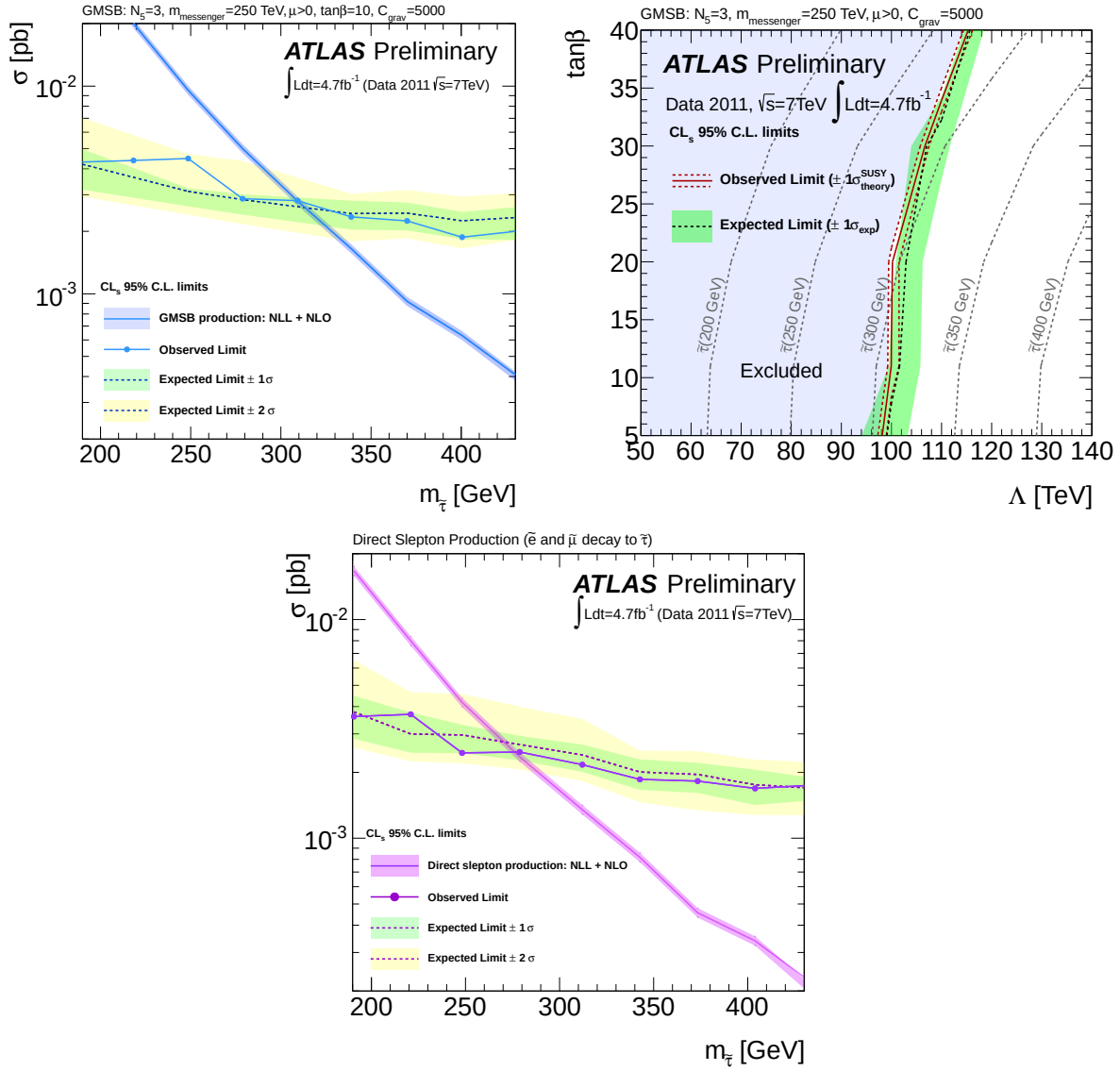

Figure 4: Mass limits on the $\tilde{\tau}$ in GMSB models (top-left), limits on Λ and $\tan\beta$ in GMSB models (top-right) and the mass limit on directly produced sleptons (bottom). In the top-left and bottom plots expected limits are drawn as dashed lines with ± 1 and $\pm 2\sigma$ uncertainty bands drawn in green and yellow repectively. Observed limits are given as solid lines with markers. The theoretical prediction for the cross-section is shown as a single line with a coloured 1σ band. In the top-right plot the expected limit is drawn as a dashed black line with green 1σ band while the observed limit is a solid red line with the 1σ theoretical uncertainty bounded by red dashed lines.

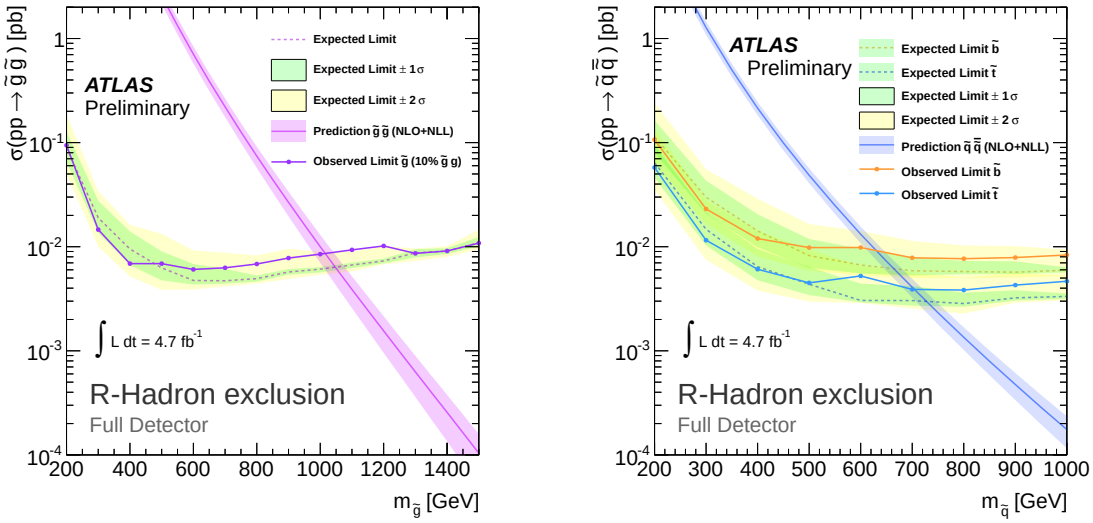

Figure 5: Cross-section exclusion limits for both gluino and squark *R*-hadrons using the full detector reconstruction are shown as the expected limit (dashed line) with ±1 and ±2σ uncertainty bands (green and yellow bands respectively) and the observed upper limit (solid line with markers). In the squark plot sbottom limits are drawn in red while stop limits are blue. The solid, rapidly sloping line is the theoretical prediction for the production cross-section calculated at NLO+NLL.

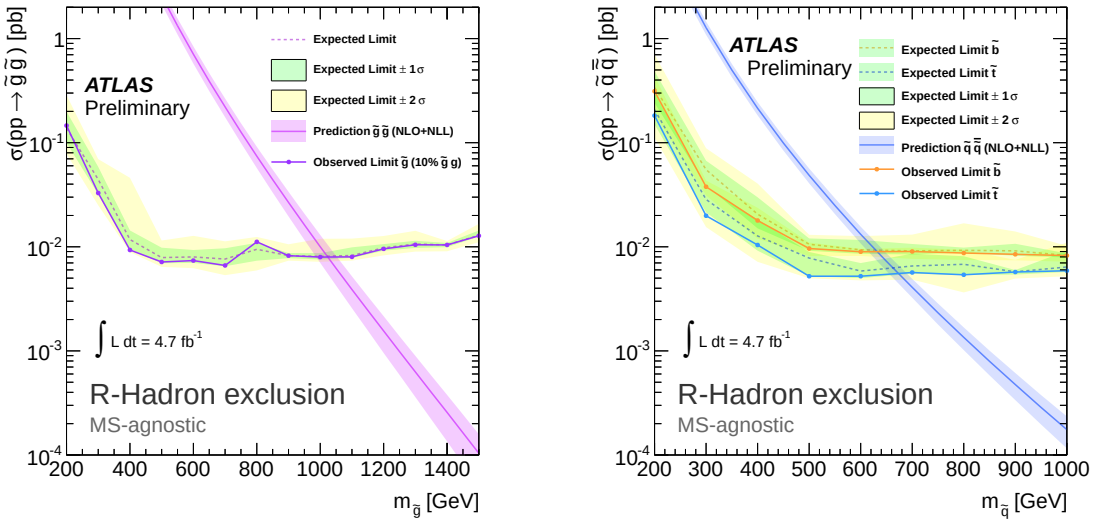

Figure 6: Cross-section exclusion limits for both gluino and squark *R*-hadrons which are neutral in the muon spectrometer. Colours and lines are as in Figure 5.

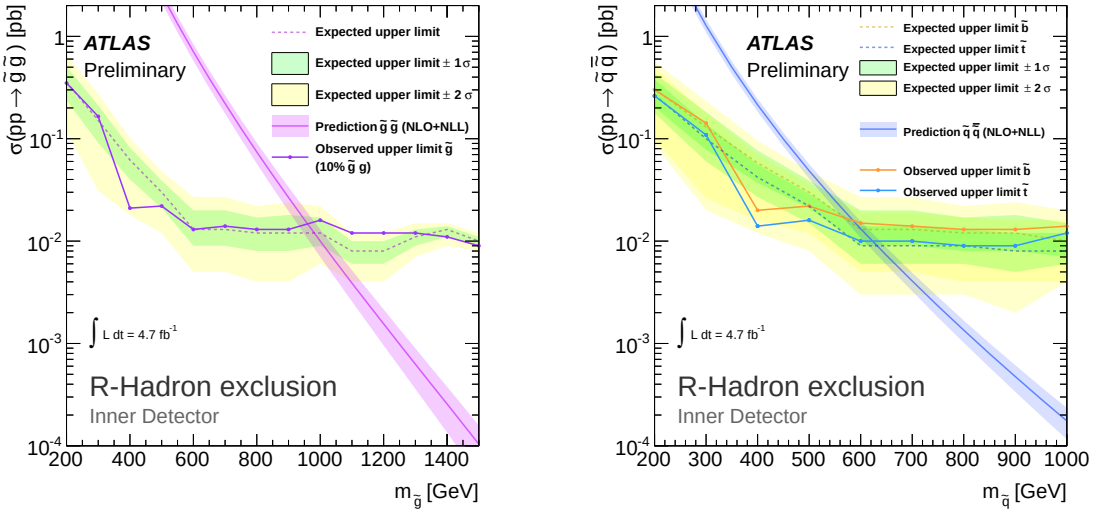

Figure 7: Cross-section exclusion limits for gluino (left) and squark (right) *R*-hadrons with a short lifetime (>10 ns) using only the inner detector. Colours and lines are as in Figure 5.

References

[1] H. Miyazawa, *Baryon Number Changing Currents*, Prog. Theor. Phys. **36 (6)** (1966) 1266–1276.

[2] P. Ramond, *Dual Theory for Free Fermions*, Phys. Rev. **D3** (1971) 2415–2418.

[3] Y. A. Gol'fand and E. P. Likhtman, *Extension of the Algebra of Poincare Group Generators and Violation of p Invariance*, JETP Lett. **13** (1971) 323–326. [Pisma Zh.Eksp.Teor.Fiz.13:452-455,1971].

[4] A. Neveu and J. H. Schwarz, *Factorizable dual model of pions*, Nucl. Phys. **B31** (1971) 86–112.

[5] A. Neveu and J. H. Schwarz, *Quark Model of Dual Pions*, Phys. Rev. **D4** (1971) 1109–1111.

[6] J. Gervais and B. Sakita, *Field theory interpretation of supergauges in dual models*, Nucl. Phys. **B34** (1971) 632–639.

[7] D. V. Volkov and V. P. Akulov, *Is the Neutrino a Goldstone Particle?*, Phys. Lett. **B46** (1973) 109–110.

[8] J. Wess and B. Zumino, *A Lagrangian Model Invariant Under Supergauge Transformations*, Phys. Lett. **B49** (1974) 52.

[9] J. Wess and B. Zumino, *Supergauge Transformations in Four-Dimensions*, Nucl. Phys. **B70** (1974) 39–50.

[10] M. Dine and W. Fischler, *A Phenomenological Model of Particle Physics Based on Supersymmetry*, Phys. Lett. **B110** (1982) 227.

[11] L. Alvarez-Gaume, M. Claudson, and M. B. Wise, *Low-Energy Supersymmetry*, Nucl. Phys. **B207** (1982) 96.

[12] C. R. Nappi and B. A. Ovrut, *Supersymmetric Extension of the SU(3) x SU(2) x U(1) Model*, Phys. Lett. **B113** (1982) 175.

[13] M. Dine and A. E. Nelson, *Dynamical supersymmetry breaking at low-energies*, Phys. Rev. **D48** (1993) 1277–1287, arXiv:hep-ph/9303230.

[14] M. Dine, A. E. Nelson, and Y. Shirman, *Low-energy dynamical supersymmetry breaking simplified*, Phys. Rev. **D51** (1995) 1362–1370, arXiv:hep-ph/9408384.

[15] M. Dine, A. E. Nelson, Y. Nir, and Y. Shirman, *New tools for low-energy dynamical supersymmetry breaking*, Phys. Rev. **D53** (1996) 2658–2669, arXiv:hep-ph/9507378.

[16] C. F. Kolda, *Gauge-mediated supersymmetry breaking: Introduction, review and update*, Nucl. Phys. Proc. Suppl. **62** (1998) 266–275, arXiv:hep-ph/9707450.

[17] ALEPH Collaboration, R. Barate et al., *Search for pair production of longlived heavy charged particles in e^+e^- annihilation*, Phys.Lett. **B405** (1997) 379–388, arXiv:hep-ex/9706013 [hep-ex].

[18] DELPHI Collaboration, P. Abreu et al., *Search for heavy stable and longlived particles in e^+e^- collisions at $\sqrt{s}$ = 189 GeV*, Phys.Lett. **B478** (2000) 65–72, arXiv:hep-ex/0103038 [hep-ex].

[19] L3 Collaboration, P. Achard et al., *Search for heavy neutral and charged leptons in e^+e^- annihilation at LEP*, Phys.Lett. **B517** (2001) 75–85, arXiv:hep-ex/0107015 [hep-ex].

[20] OPAL Collaboration, G. Abbiendi et al., *Search for stable and longlived massive charged particles in e^+e^- collisions at $\sqrt{s}$ = 130 GeV to 209* GeV, Phys.Lett. **B572** (2003) 8–20, arXiv:hep-ex/0305031 [hep-ex].

[21] H1 Collaboration, A. Aktas et al., *Measurement of anti-deuteron photoproduction and a search for heavy stable charged particles at HERA*, Eur.Phys.J. **C36** (2004) 413–423, arXiv:hep-ex/0403056 [hep-ex].

[22] CDF Collaboration, F. Abe et al., *Search for Heavy Stable Particles at the Fermilab Collider*, Phys.Rev.Lett. **63** (1989) 1447.

[23] CDF Collaboration, F. Abe et al., *Limits on the production of massive stable charged particles*, Phys.Rev. **D46** (1992) 1889–1894.

[24] CDF Collaboration, D. Acosta et al., *Search for long-lived charged massive particles in $\bar{p}p$ collisions at $\sqrt{s}$ = 1.8 TeV*, Phys.Rev.Lett. **90** (2003) 131801, arXiv:hep-ex/0211064 [hep-ex].

[25] D0 Collaboration, V. M. Abazov et al., *Search for Stopped Gluinos from $p\overline{p}$ Collisions at $\sqrt{s}$ = 1.96 TeV*, Phys. Rev. Lett. **99** (2007) 131801. http://link.aps.org/doi/10.1103/PhysRevLett.99.131801.

[26] D0 Collaboration, V. Abazov et al., *Search for Long-Lived Charged Massive Particles with the D0 Detector*, Phys.Rev.Lett. **102** (2009) 161802, arXiv:0809.4472 [hep-ex].

[27] CDF Collaboration, T. Aaltonen et al., *Search for Long-Lived Massive Charged Particles in 1.96 TeV $\bar{p}p$ Collisions*, Phys.Rev.Lett. **103** (2009) 021802, arXiv:0902.1266 [hep-ex].

[28] D0 Collaboration, V. M. Abazov et al., *Search for Charged Massive Long-Lived Particles*, Phys. Rev. Lett. **108** (2012) 121802. http://link.aps.org/doi/10.1103/PhysRevLett.108.121802.

[29] CMS Collaboration, *Search for Stopped Gluinos in pp collisions at $\sqrt{s}$ = 7 TeV*, Phys.Rev.Lett. **106** (2011) 011801, arXiv:1011.5861 [hep-ex].

[30] CMS Collaboration, *Search for Heavy Stable Charged Particles in pp collisions at $\sqrt{s}$ = 7 TeV*, JHEP **1103** (2011) 024, arXiv:1101.1645 [hep-ex].

[31] ATLAS Collaboration, *Search for Massive Long-lived Highly Ionising Particles with the ATLAS Detector at the LHC*, Phys.Lett. **B698** (2011) 353–370, arXiv:1102.0459 [hep-ex].

[32] ATLAS Collaboration, *Search for stable hadronising squarks and gluinos with the ATLAS experiment at the LHC*, Phys.Lett. **B701** (2011) 1–19, arXiv:1103.1984 [hep-ex].

[33] ATLAS Collaboration, *Search for Heavy Long-Lived Charged Particles with the ATLAS detector in pp collisions at $\sqrt{s}$ = 7 TeV*, Phys.Lett. **B703** (2011) 428–446, arXiv:1106.4495 [hep-ex].

[34] ATLAS Collaboration, *Search for decays of stopped, long-lived particles from 7 TeV pp collisions with the ATLAS detector*, Eur.Phys.J. **C72** (2012) 1965, arXiv:1201.5595 [hep-ex].

[35] CMS Collaboration, *Search for heavy long-lived charged particles in pp collisions at $\sqrt{s}$ = 7 TeV*, arXiv:1205.0272 [hep-ex].

[36] L. W. Nagel and D. Pederson, *SPICE (Simulation Program with Integrated Circuit Emphasis)*, . http://www.eecs.berkeley.edu/Pubs/TechRpts/1973/22871.html.

[37] G. Corcella et al., *HERWIG 6.5: an event generator for Hadron Emission Reactions With Interfering Gluons (including supersymmetric processes)*, JHEP **01** (2001) 010, arXiv:hep-ph/0011363.

[38] T. Sjostrand, S. Mrenna, and P. Skands, *PYTHIA 6.4 Physics and Manual*, JHEP **05** (2006) 026, arXiv:hep-ph/0603175.

[39] The source code for the dedicated R-hadron hadronisation routines can be downloaded from: http://home.thep.lu.se/~torbjorn/pythiaaux/recent.html.

[40] A. C. Kraan, *Interactions of heavy stable hadronizing particles*, Eur. Phys. J. **C37** (2004) 91–104, arXiv:hep-ex/0404001.

[41] G. Farrar, R. Mackeprang, D. Milstead, and J. Roberts, *Limit on the mass of a long-lived or stable gluino*, JHEP **1102** (2011) 018, arXiv:1011.2964 [hep-ph].

[42] GEANT4 Collaboration, S. Agostinelli et al., *GEANT4: A simulation toolkit*, Nucl. Instrum. Meth. **A506** (2003) 250–303.

[43] http://r-hadrons.web.cern.ch/r-hadrons/.

[44] R. Mackeprang and D. Milstead, *An Updated Description of Heavy-Hadron Interactions*, arXiv:0908.1868 [hep-ph].

[45] C. Alexa, S. Constantinescu, and S. Dita, *Geant4 hadronic physics validation with ATLAS tile calorimeter test-beam data*, AIP Conf. Proc. **867** (2006) 463–470.

[46] ATLAS Collaboration, *The ATLAS Experiment at the CERN Large Hadron Collider*, JINST **3** (2008) S08003.

[47] ATLAS Collaboration, *dE/dx measurement in the ATLAS Pixel Detector and its use for particle identification*, ATLAS-CONF-2011-016 (2011) .

[48] ATLAS Collaboration, *Expected Performance of the ATLAS Experiment - Detector, Trigger and Physics*, arXiv:0901.0512 [hep-ex].

[49] T. Matsushita, *Performance of the ATLAS muon trigger in 2011*, ATL-DAQ-PROC-2012-008 .

[50] G. Cacciari, G. P. Salam, and G. Soyez, *The anti-k_t jet clustering algorithm*, JHEP **04** (2008) 063, arXiv:0802.1189.

[51] H. Bichsel, *Straggling in thin silicon detectors*, Rev. Mod. Phys. **60** (1988) 663–699. http://link.aps.org/doi/10.1103/RevModPhys.60.663.

[52] W. Beenakker, M. Kramer, T. Plehn, M. Spira, and P. M. Zerwas, *Stop production at hadron colliders*, Nucl. Phys. **B515** (1998) 3–14, hep-ph/9710451.

[53] W. Beenakker, S. Brensing, M. Kramer, A. Kulesza, E. Laenen, and I. Niessen, *Supersymmetric top and bottom squark production at hadron colliders*, JHEP. **1008** (2010) 098, arXiv:1006.4771 [hep-ph].

[54] W. Beenakker, S. Brensing, M. Kramer, A. Kulesza, E. Laenen, et al., *Squark and gluino hadroproduction*, Int.J.Mod.Phys. **A26** (2011) 2637–2664, arXiv:1105.1110 [hep-ph].

[55] W. Beenakker, R. Hopker, M. Spira, and P. M. Zerwas, *Squark and gluino production at hadron colliders*, Nucl. Phys. **B492** (1997) 51–103, arXiv:hep-ph/9610490.

[56] M. Kramer, A. Kulesza, R. van der Leeuw, M. Mangano, S. Padhi, et al., *Supersymmetry production cross sections in pp collisions at sqrts = 7 TeV*, arXiv:1206.2892 [hep-ph].

[57] P. Z. Skands, *Tuning Monte Carlo Generators: The Perugia Tunes*, Phys. Rev. **D82** (2010) 074018, arXiv:1005.3457 [hep-ph].

[58] ATLAS Collaboration Collaboration, *Jet energy scale and its systematic uncertainty in proton-proton collisions at sqrt(s)=7 TeV in ATLAS 2010 data*, ATLAS-CONF-2011-032, available at http://cdsweb.cern.ch/record/1337782 (2011) .

[59] *Muon reconstruction efficiency in reprocessed 2010 LHC proton-proton collision data recorded with the ATLAS detector*, Tech. Rep. ATLAS-CONF-2011-063, CERN, Geneva, Apr, 2011.

[60] ATLAS Collaboration, *Luminosity Determination in pp Collisions at sqrt(s) = 7 TeV using the ATLAS Detector in 2011*, ATLAS-CONF-2011-116 (2011) .

[61] ATLAS Collaboration, *Luminosity Determination in pp Collisions at sqrt(s)=7 TeV using the ATLAS Detector at the LHC*, Eur. Phys. J. C **71** (2011) 1630, arXiv:1101.2185.

[62] A. L. Read, *Presentation of search results: the CL_s technique*, Journal of Physics G **28** (2002) 2693.